The Astrophysical Journal Letters, 886:L5 (8pp), 2019 November 20 https://doi.org/10.3847/2041-8213/ab53ed

An Ongoing Mid-infrared Outburst in the White Dwarf 0145+234: Catching in Action the Tidal Disruption of an Exoasteroid?

Ting-gui Wang[1,2], Ning Jiang[1,2], Jian Ge[3], Roc M. Cutri[4], Peng Jiang[5], Zhengfeng Sheng[1,2], Hongyan Zhou[1,5], James Bauer[6], Amy Mainzer[7], and Edward L. Wright[8]

[1] CAS Key Laboratory for Researches in Galaxies and Cosmology, University of Sciences and Technology of China, Hefei, Anhui 230026, People's Republic of China; twang@ustc.edu.cn
[2] School of Astronomy and Space Sciences, University of Science and Technology of China, Hefei, 230026, People's Republic of China
[3] 211 Bryant Space Science Center, Department of Astronomy, University of Florida, Gainesville, FL 32611-2055, USA
[4] IPAC/Caltech, 1200 E. California Boulevard, Pasadena, CA 91125, USA
[5] Antarctic Astronomy Research Division, Key Laboratory for Polar Science of the State Oceanic Administration, Polar Research Institute of China, Shanghai, People's Republic of China
[6] Department of Astronomy, University of Maryland, College Park, MD 20742, USA
[7] University of Arizona, 1629 E. University Boulevard, Tucson, AZ 85721, USA
[8] Division of Astronomy and Astrophysics, University of California, Los Angeles, Los Angeles, CA 90095, USA
Received 2019 September 17; revised 2019 November 2; accepted 2019 November 4; published 2019 November 14

Abstract

We report the detection of a large-amplitude MIR outburst in the white dwarf (WD) 0145+234 in the NEOWISE Survey data. The source had a stable MIR flux before 2018, and was brightened by about 1.0 magnitude in the *W1* and *W2* bands within half a year and has been continuously brightening since then. No significant variations are found in the optical photometry data during the same period. This suggests that this MIR outburst is caused by recent replenishing or redistribution of dust, rather than intrinsic variations of the WD. Spectral energy distribution modeling of 0145+234 suggests that there was already a dust disk around the WD in the quiescent state, and both of the temperature and surface area of the disk evolved rapidly since the outburst. The dust temperature was $\simeq$1770 K in the initial rising phase, close to the sublimation temperature of silicate grains, and gradually cooled down to around 1150 K, while the surface area increased by a factor of about six during the same period. The inferred closest distance of dust to the WD is within the tidal disruption radius of a gravitationally bounded asteroid. We estimated the dust mass to be between 3×10^{15} and $3 \times 10^{17} \rho/(1\ \mathrm{g\ cm^{-3}})$ kg for silicate grains of a power-law size distribution with a high cutoff size from 0.1 to 1000 μm. We interpret this as a possible tidal breakup of an exoasteroid by the WD. Further follow-up observations of this rare event may provide insights on the origin of dust disk and metal pollution in some WDs.

Unified Astronomy Thesaurus concepts: White dwarf stars (1799); Circumstellar dust (236); Infrared excess (788); Variable radiation sources (1759)

1. Introduction

A substantial fraction of white dwarfs (WDs) are known to show metal absorption lines in their spectra (Zuckerman et al. 2010; Koester et al. 2014). Because heavy elements diffuse out of the photosphere in a rather short time (days to hundred years, depending on $T_{\rm eff}$ and $\log g$) in the strong surface gravity of a WD[9] (Koester 2009; Bergeron et al. 2015), this indicates that these heavy elements were added to the surface very recently, presumably, by accretion of tidally disrupted asteroids or comets (Jura & Young 2014). Many WDs also display infrared excesses, which may be considered as evidence for dust disks (Zuckerman & Becklin 1987; Farihi et al. 2009; Rebassa-Mansergas et al. 2019). The presence of a warm disk is further supported by the detection of double-peaked infrared Ca II emission lines (Jura 2003; Gänsicke et al. 2006; Veras et al. 2014). Dust in the disk in a WD is either transient or continuously replenished because grains can be dragged onto the star through the Poynting–Robertson force on timescales of several years (e.g., Reach et al. 2005; Rafikov 2011). Fragmentation of a planetary body has been proposed as a source of dust (Jura & Young 2014; Vanderburg et al. 2015; Manser et al. 2019). Variability in infrared flux on a timescale from less than a year to 10 years has been reported very recently in a number of WDs (Farihi et al. 2018; Xu et al. 2018; Swan et al. 2019a), but most of variations are generally of small amplitudes (e.g., 20%–40%, Xu & Jura 2014; Xu et al. 2018; Swan et al. 2019b) on timescales of a year.

In this Letter, we report the discovery of a large MIR outburst in the WD 0145+234 (01:47:54.81 + 23:39:43.6; Wills & Wills 1974). This outburst has so far lasted one and a half years. This event was discovered during a blind search for large-amplitude MIR outbursts in the *WISE*/NEOWISE data archive (Wright et al. 2010; Mainzer et al. 2014). This could be a process of tidal disruption caught in action.

2. Data and Analysis

The *Wide-field Infrared Survey Explorer* (*WISE*) all-sky survey and NEOWISE Reactivation mission conducted repeated scans of the entire sky at 3.4 and 4.6 μm (hereafter *W1* and *W2*) beginning in 2010 January through the present, except for the period 2011 February–2013 November. We retrieved the *W1* and *W2* point-spread function profile-fit photometry of 0145+234 from the AllWISE Multi-epoch Photometry Table and NEOWISE-R Single Exposure (L1b)

[9] http://montrealwhitedwarfdatabase.org/evolution.html

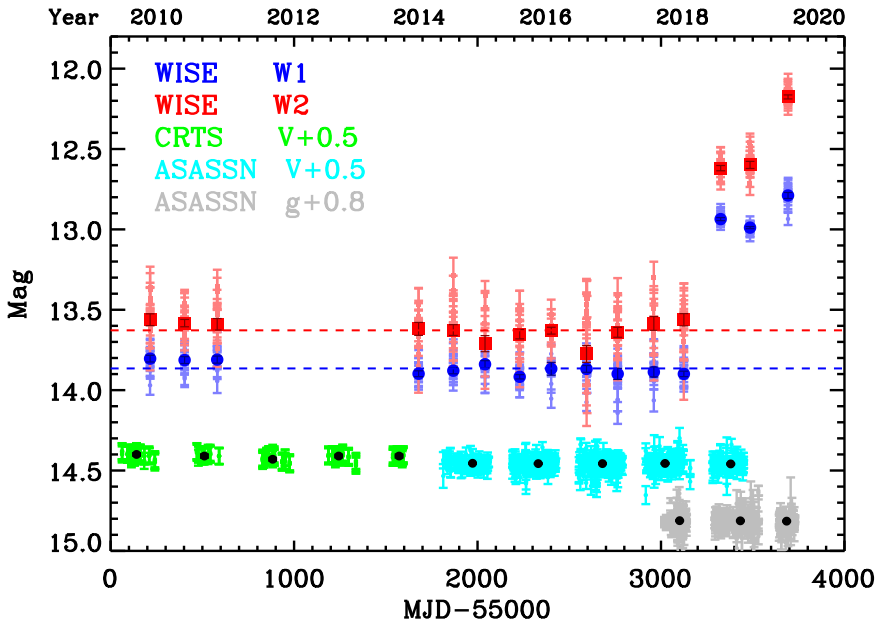

Figure 1. *WISE*/NEOWISE(-R) and optical light curves of the white dwarf 0145+234. Legend: blue circles and red squares are the epoch medians of *W1* and *W2* magnitude. Black circles are median magnitudes in *V* or *g* over one observational season.

Source Table,[10] which contain all measurements from 2010 to 2019 July. The single-exposure data were first screened by the quality flag marked in the catalogs to remove measurements with poor quality or possible corruption: ($qual\_frame < 5$), charged particle hits ($saa\_sep < 5$), scattered moon light ($moon\_masked = 1$), and artifacts ($cc\_flags > 0$). The high-quality measurements in each six-month observation epoch were averaged to increase the signal-to-noise ratio of the photometry, resulting in 15 epochs (see Figure 1). No significant variations are present in the first 12 epochs and thus we take them as the quiescent state with average magnitudes of 13.87 ± 0.04 and 13.63 ± 0.06 in the *W1* and *W2* bands, respectively. The light curve displays a large outburst between the 2018 January and 2018 July epochs ($\Delta W1 = 0.93 \pm 0.04$, $\Delta W2 = 1.01 \pm 0.06$) and continues rising in the later epochs. Overall, the outburst appears to display a redder-when-brighter trend in which the variation amplitude in the *W2* band is larger than that in the *W1* band.

The brightening of 0145+234 is not the result of object's motion carrying it close to a bright nearby source. The proper motion of the WD is measured by *Gaia* to be $\mu_{\rm R.A.} = -5.21 \pm 0.12$ and $\mu_{\rm decl.} = -97.59 \pm 0.08$ mas year^{-1} (Gaia Collaboration et al. 2018). Examination of the AllWISE Atlas Image (epoch 2010) shows that the closest MIR source is approximately 14″ to the southwest of the WD position. The nearby source was cleanly separated and measured in the AllWISE Catalog, and is 1.6 mag fainter in *W1* and *W2* than J0145+234 in 2010. Even if the WD moved directly onto that source, which it did not (see Figures 2 and 3), the apparent flux increase would be much too small to account for the brightening observed in the light curve.

The relative motion of 0145+234 is clearly detected from the AllWISE and NEOWISE astrometry that spans a time baseline of 9 yr and is fully consistent with proper motion measured by *Gaia*, as illustrated in Figure 4. The position of the white dwarf during outburst does not show any deviation from the expected motion larger than 0.″1. Thus, a chance coincidence with a bright nearby source could not have shifted the photocenter of the WD, making this occurrence unlikely.

W1 and *W2* images comparing the region around 0145+234 in 2014 January, 2018 January, and 2019 January are shown in Figures 2 and 3. The 2014 January and 2018 images are pre-outburst, and the difference images between the 2018 and 2014 show only a very small positive/negative residual due to the slight motion of the source in the four years separating the observations. The differences between the 2019 and 2014 images show a bright, pointlike image at the position of the WD that is the source in outburst.

0145+234 is bright in the optical band ($V \sim 13.93$ mag) and thus has been well measured by various optical time-domain surveys. We retrieved the optical photometry data from the publicly released data archive from the Catalina Real-time Transient Survey [11] (CRTS; Drake et al. 2009) and All-Sky Automated Survey for Supernovae (ASAS-SN; Shappee et al. 2014; Kochanek et al. 2017).[12] The CRTS survey has monitored 0145+234 since 2005 without filters, but the photometry is calibrated to a pseudo-*V* magnitude using a few dozen preselected standard stars in each field. The public CRTS data are available to 2013 October. Fortunately, the public ASAS-SN survey can serve the subsequent *V*-band photometry. Although the latest observations are performed in the *g* band, these *g*-band data largely overlap with *V*-band data. In contrast to the remarkable MIR variability, 0145+234 is quite stable and shows negligible variability in the long-term (more than one decade) optical light curves, including the MIR outburst period.

We made the quiescent spectral energy distribution (SED) of the WD by collecting data from *GALEX*, PANSTARRs (Chambers et al. 2016), *Gaia* (Gaia Collaboration et al. 2016), 2MASS (Skrutskie et al. 2006), and ALLWISE. We matched the UV to near-infrared photometry with the synthesized WD SED

[10] https://irsa.ipac.caltech.edu/cgi-bin/Gator/nph-scan?mission=irsa&submit=Select&projshort=WISE

[11] http://nunuku.caltech.edu/cgi-bin/getcssconedb_release_img.cgi

[12] https://asas-sn.osu.edu/

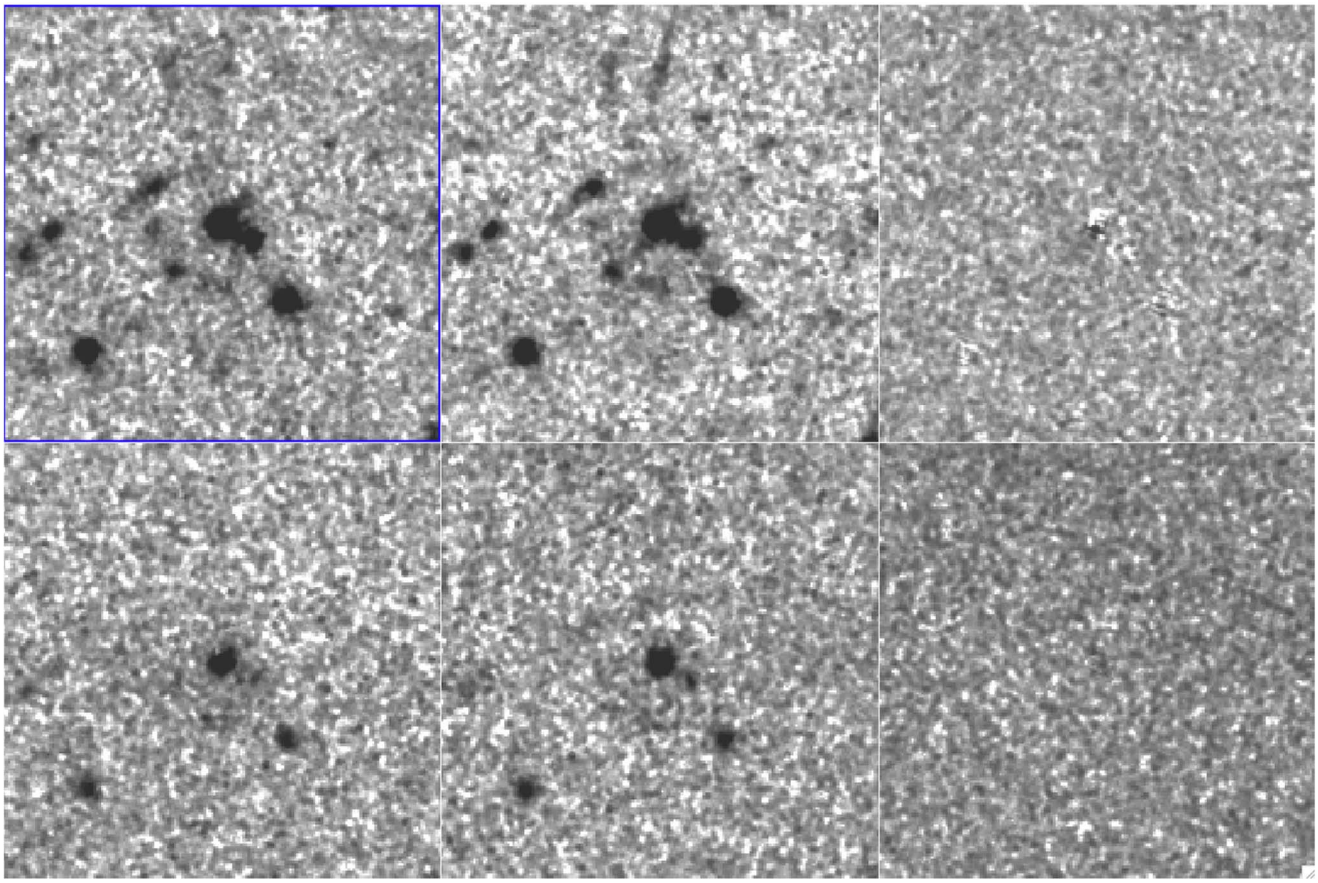

Figure 2. Top panels: montage of *W1* images showing a 180″ × 180″ region centered on the position of 0145+234 from the AllWISE Catalog. The left panel shows the coaddition of the 2014 January single exposures, the center panel is the coaddition of the 2018 January single exposures, and the right panel is the difference between the 2018 and 2014 January images. Bottom panels: same as the top panels, but for *W2*.

models (Figure 5).[13] The models cover the range of $T_{\rm eff}$ from 2500 K to 90,000 K and log g from 7.0 to 9.0 with a step of 0.5 for DA WDs, and $T_{\rm eff}$ from 3250 K to 70,000 K and log g from 7.0 to 9.0 for DB WDs (Bergeron et al. 2011; Tremblay et al. 2011; Blouin et al. 2018). The interstellar reddening of the CCM law with $R_V = 3.1$ (Cardelli et al. 1989) was added with the $E(B-V)$ as a free parameter. The best-fitted parameters converge to a model $T_{\rm eff} = 13{,}000$ K, log $g = 8.0$, and $E(B-V) = 0.014 \pm 0.004$. They are consistent with those derived from the spectroscopic model ($T = 13{,}060 \pm 217$ K, log $g = 8.13 \pm 0.05$, Gianninas et al. 2011; $T = 12{,}910 \pm 219$ K, log $g = 8.11 \pm 0.05$, Limoges et al. 2015). There is no evidence for a stellar companion for this WD either from broadband SEDs (Figure 5) or the optical spectrum. We examined their optical spectrum in the Montreal WD database,[14] and found an absorption line of Ca II 3934. Unfortunately, Ca II 3969 is difficult to identify because it falls in the absorption trough of a Balmer absorption line. This suggests it is a DAZ WD. With these photospheric parameters, we also derived other parameters of the WD[15] (Fontaine et al. 2001; Gianninas et al. 2011): the mass of $M_* = 0.667\,M_\odot$, the radius of $R_{\rm WD} = 0.0116\,R_\odot$, the luminosity of $L_{\rm WD} = 0.00350\,L_\odot$, and the age of 0.381 Gyr.

[13] http://www.astro.umontreal.ca/~bergeron/CoolingModels

[14] http://montrealwhitedwarfdatabase.org/WDs/WD%200145+234/WD%200145+234.html

[15] http://montrealwhitedwarfdatabase.org/evolution.html

2.1. IR Excess in the Low State

The observed ALLWISE fluxes in the *W1*, *W2*, and *W3* (12 μm) bands are clearly above the predicted values from the WD model (Figure 5). The excess over WD photospheric emission are significant at about 10σ in the *W1* and *W2* bands, and 9σ in the *W3* band. The infrared excess indicates a dust disk. Initially, we added a blackbody curve to model the infrared excess, and found that it is insufficient to fit all the data with a 2σ excess in the *W3* band, which requires an additional temperature component or the non-gray dust model to fit. However, since a two-component model needs a total of four parameters (two temperatures and two surface areas), while only three data points (*W1*, *W2*, and *W3*) are available, such a model cannot be fully constrained. To illustrate the possibility of non-gray dust model, we adopt the particle-cluster-aggregation (PCA) model for olivine (Nakamura 1998), which is used to explain the scattering disk of β Pic. Without increasing the number of free parameters, the model can now fit the data (Figure 5).

2.2. Dust in the High State

In the high state, this source is more than one magnitude brighter in the *W1* and *W2* bands. Since we only have two data points, we chose to fit the MIR excess with a single-temperature blackbody model. We considered two different scenarios: (1) the quiescent dust disk has been transformed into the latter one; (2) the quiescent disk remains the same and there

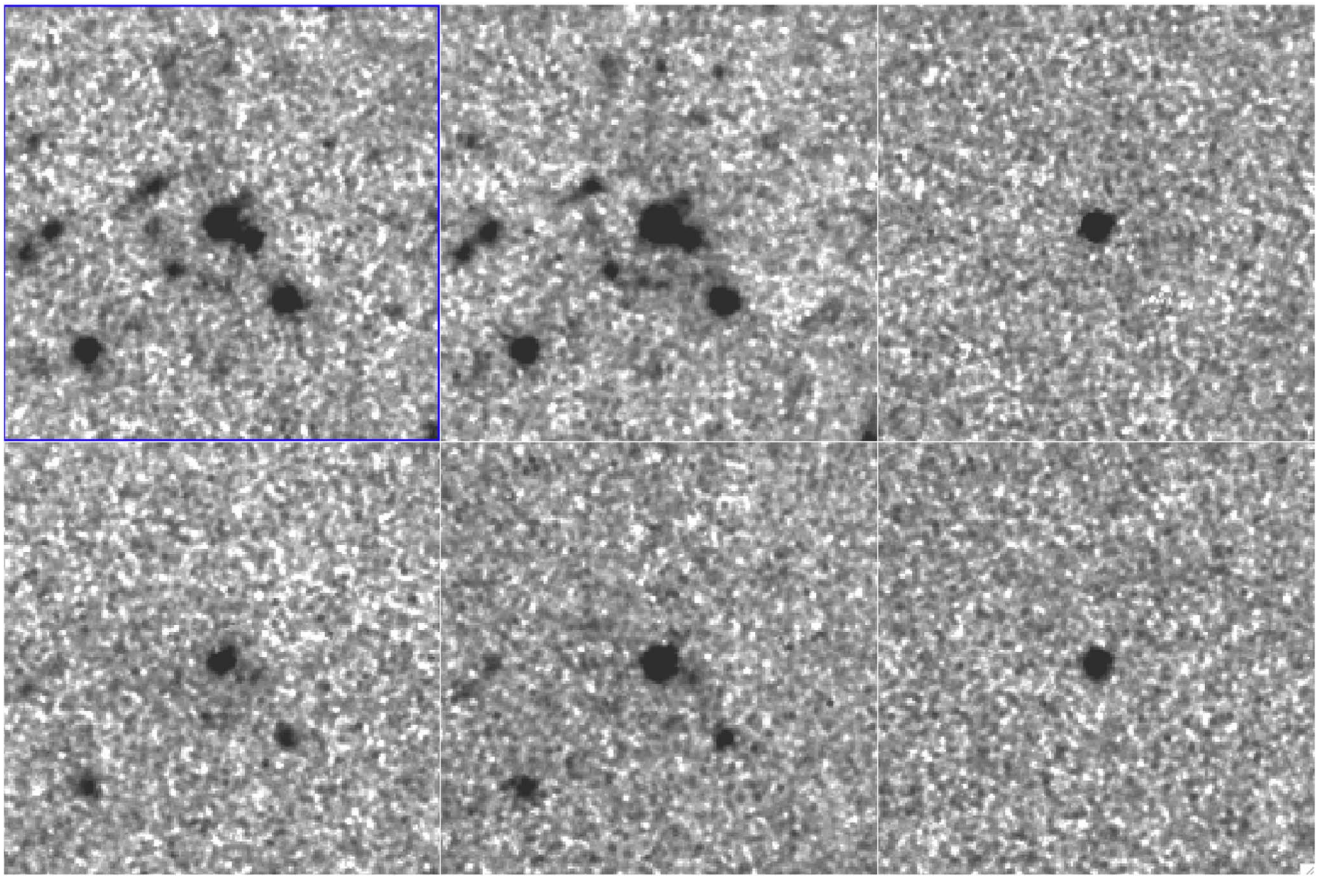

Figure 3. Top panels: montage of *W1* images showing a 180″ × 180″ region centered on the position of 0145+234 from the AllWISE Catalog. The left panel shows the coaddition of the 2014 January single exposures, the center panel is the coaddition of the 2019 January single exposures when the source was in outburst, and the right panel is the difference between the 2019 January and 2014 January images. Bottom panels: same as the top panels, but for *W2*.

Table 1
Blackbody Model Fit to the MIR Excess

Epoch	*W1*	*W2*	Scenario 1[a]			Scenario 2[b]		
			T	*A*	*R*	*T*	*A*	*R*
	(mag)	(mag)	(K)	(10^{16} m^2)	$(R)_\odot$	K	10^{16} m^2	$R_\odot$
1–12	13.87 ± 0.04	13.63 ± 0.06	1163 ± 145	3.54 ± 1.50	1.46 ± 0.37	…	…	…
13	12.94 ± 0.01	12.62 ± 0.02	1769 ± 74	4.80 ± 0.51	0.63 ± 0.05	1949 ± 529	2.99 ± 1.88	0.52 ± 0.28
14	12.99 ± 0.01	12.60 ± 0.02	1515 ± 62	6.96 ± 0.84	0.88 ± 0.07	1570 ± 329	4.89 ± 2.77	0.80 ± 0.34
15	12.79 ± 0.02	12.18 ± 0.01	1146 ± 32	23.06 ± 2.08	1.52 ± 0.09	1115 ± 130	21.34 ± 8.80	1.59 ± 0.37

Notes.
[a] Fitting excesses to the WD model.
[b] Fitting quiescent state subtracted MIR flux.

is a new dust component that contributes to the brightening of the source. In the first case, we fit the total observed excess in the *W1* and *W2* bands at high state with a blackbody model. In the second case, we only fit the varying *W1* and *W2* fluxes with a blackbody model to constrain the newly formed dust component. The varying fluxes were calculated by subtraction of the mean quiescent flux from the high state fluxes, and uncertainties were calculated through propagations of errors. These results are summarized in Table 1 (see also Figure 5). In the first case, the temperature was increased from 1163 K to 1769 K from quiescent epochs (1–12) to epoch 13, while the surface area might be increased but the large uncertainties in the quiescent state make this inconclusive. In the subsequent epochs, the dust temperature is decreased continuously to 1146 K at the last epoch, while the surface area increases by a factor of about four. In the second case, the newly formed dust had an initial temperature of about 1950 K, and decreased to 1115 K at the last epoch, while surface area increased by a factor of about six.

With the above fit parameters, we can estimate physical quantities of the dust. The distance to the WD is 29.458 ± 0.044 pc using the parallax from the *Gaia* DR2 data (Gaia Collaboration et al. 2016, 2018; Lindegren et al. 2018), which is consistent with that derived from the SED fitting. We adopted the bolometric luminosity of 0.0035 $L_\odot$ and WD radius of 0.0116 $R_\odot$ from the spectroscopic WD model[16] (Fontaine et al. 2001;

[16] http://montrealwhitedwarfdatabase.org/evolution.html

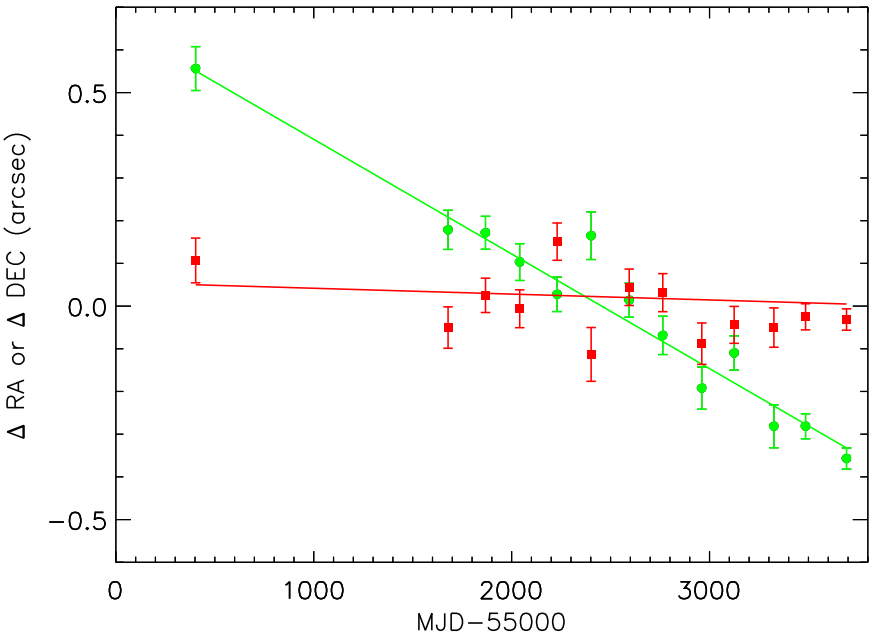

Figure 4. Relative R.A. (in red) and decl. (in green) motion of the MIR source with respect to their mean values during the *WISE*/NEOWISE surveys. The earliest points are from the AllWISE Catalog and represent the average positions from the 2010 January, 2010 July, and 2011 January measurement epochs. The points following MJD = 55600 are the average positions measured during each six-month NEOWISE observation epoch. For comparison, the solid red and green lines show the expected R.A. and decl. motion of the white dwarf based on the *Gaia* astrometry and proper motion.

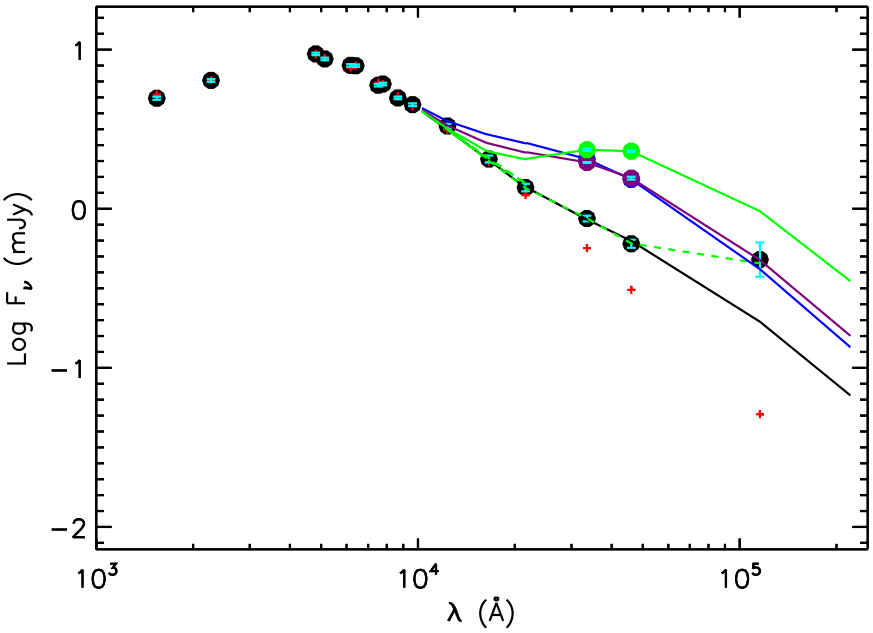

Figure 5. Spectral energy distribution (circles with error bars in cyan) and best-fitted models (cross or solid curve). The black, blue, purple, and green symbols represent the observed data on epochs 1–12, 13, 14, and 15 in the light curve, respectively (see Table 1). The WD photosphere model is represented by red crosses. The solid curves represent the blackbody fit to the excesses over the WD photosphere model (colors follow the symbols). The PCA dust model is shown as the dashed green curve.

Gianninas et al. 2011). Assuming the dust is gray and in thermal equilibrium, we estimated the distance to the central star is on the order of

$$R_{\rm dust} = \left(\frac{L_{\rm WD}}{4\pi\sigma T_d^4}\right)^{1/2} = (T_{\rm eff}/T_d)^2 R_{\rm WD}. \quad (1)$$

The distances of the dust to the WD are also listed in Table 1. The closest distance to the WD is about 0.5 $R_\odot$.

The covering factor of the dust can be estimated from the ratio of the blackbody luminosity to the WD luminosity assuming dust is optically thick to the UV to optical light of the WD. The covering factor in the high state sharply rises to around $(1.5-2.0)\times10^{-2}$ from $(2.7\pm0.3)\times10^{-3}$ in the quiescent state, and remains nearly constant in the last three epochs.

Real dust is likely not gray, so the derived temperature and dust mass depends on the size distribution of grains ($N(a)$) and

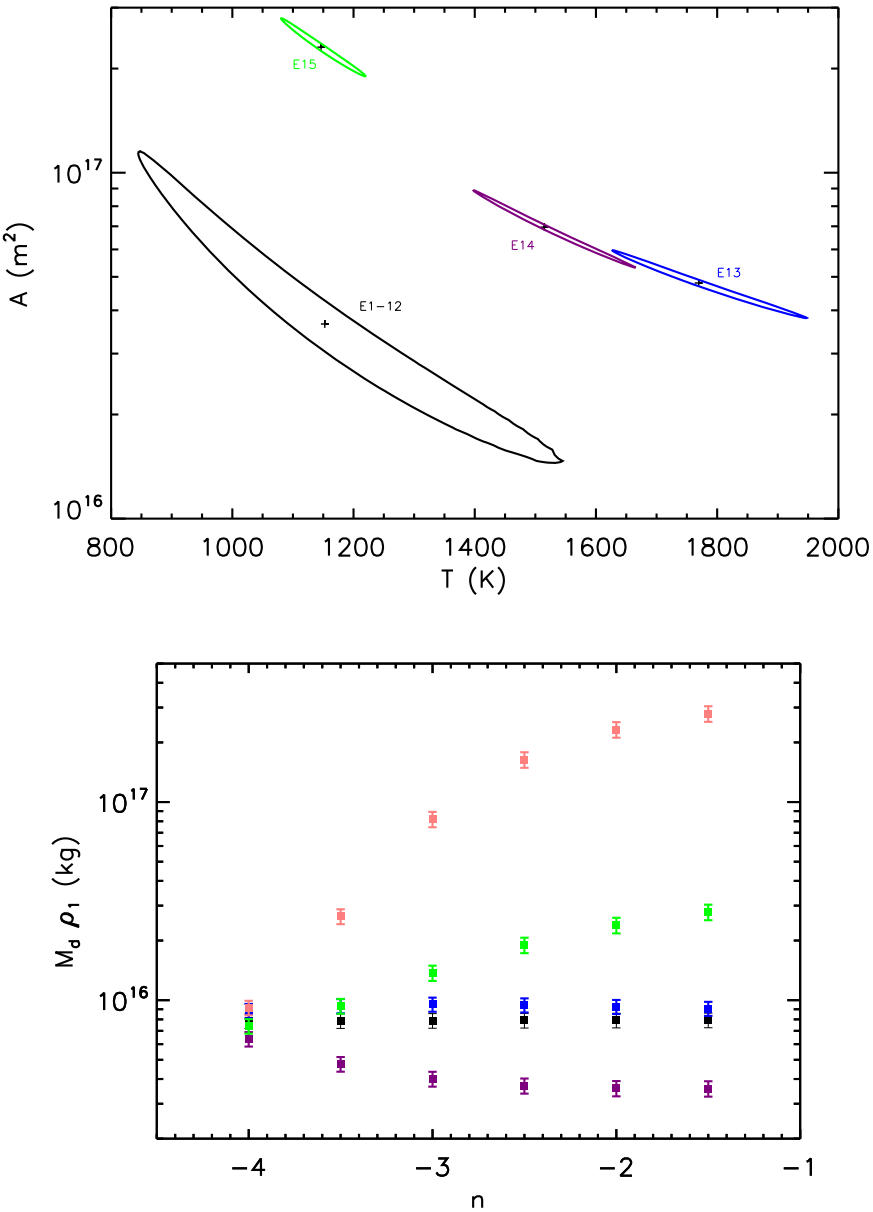

Figure 6. Upper panel: 90% contours for the blackbody fit to the excess IR flux on four epochs. The best-fitted parameters are marked as crosses. Colors are the same as those in Figure 5. Lower panel: the fitted dust mass of silicate grains as a function of power-law index at different cutoff of the largest grain size (red: 1000, green: 100, blue: 10, black: 1, and purple: 0.1 μm) for the last epoch of the NEOWISE-R survey.

their absorption coefficients (Q). In the following, we assume that the sizes of dust grains follow a power-law distribution with an index n in the range from $a_{\rm min}$ to $a_{\rm max}$ and none outside the range. The dust emission flux can be estimated

$$f_\nu = \int_{a_{\rm min}}^{a_{\rm max}} N(a) 4\pi a^2 Q_\nu(a) da \pi B_\nu(T) \Big/ (4\pi d_L^2) = \frac{3M_d}{4\rho d_L^2} \left\langle \frac{Q_\nu}{a} \right\rangle B_\nu(T), \quad (2)$$

where

$$\left\langle \frac{Q_\nu}{a} \right\rangle = \frac{\int_{a_{\rm min}}^{a_{\rm max}} N(a) a^3 (Q/a) da}{\int_{a_{\rm min}}^{a_{\rm max}} N(a) a^3 da}, \quad (3)$$

and M_d, ρ are the mass and density of the dust, respectively. The d_L is the distance to the WD. In the blackbody case, the absorption coefficient is $Q_\nu = 1$.

Using silicate coefficients[17] in Laor & Draine (1993), we calculated a set of $\left\langle \frac{Q_\nu}{a} \right\rangle$ for $a_{\rm min} = 0.01$ μm and $a_{\rm max} = 0.1$, 1, 10, 100, 1000 μm. The excess infrared emission is then fitted with each of above models to derive mass and temperature of the dust. The lowest derived-temperatures are $T_d = 770$, 1031, 948, 800 K for epochs 1–12, 13, 14, 15, respectively, or 60%–70% of those from the blackbody model, when $n = -4$ and $a_{\rm max} = 0.1$ μm. The highest temperatures are within 99% of those from the blackbody model when $n = -1$ and $a_{\rm max} = 1000$ μm. The mass of dust is in the range of 3×10^{15} ρ_1–$3 \times 10^{17} \rho_1$ kg ($\rho_1 = \rho/(1\ {\rm g\ cm^{-3}})$), depending strongly on the size distribution (see Figure 6). A strict lower limit on the dust mass is a few times 10^{15} kg, obtained when most grains have a size of about 1 μm, which gives the maximum Q_ν/a in the *W1* and

[17] For grains of size larger than 10 μm, we set $Q_\lambda \simeq 1$ for radiation at wavelengths greater than 4 μm.

W2 bands. This minimum dust mass is very close to these of disks in the dustiest WD, e.g., 10^{15} kg in G29-38 (Reach et al. 2005) and $(0.3-1)\times 10^{15}$ kg in GD 362 (Jura et al. 2007). For a given distribution, dust mass increases monotonically with time. The increase of the amount of dust can be produced by further breakup of large bodies due to collision.

3. Discussion

The infrared light curve consists of a stable pre-burst quiescent phase, a short time rising outburst within half a year, and the MIR excess increasing phase with little variations in the optical light curve during the same period. This suggests that there is either a rapid inflow of an initial dust disk seen in the quiescent state into the inner region or tidal breakup of an asteroid into a clump of grains.

In order to understand various processes that may contribute to the dust changes, we examined the timescales of various processes, for the distance of dust to the host star of $\sim 1\,R_\odot$, the WD mass of $0.667\,M_\odot$, and the luminosity of $0.0035\,L_\odot$. First, the dynamic time, or the orbit period, is about half an hour. Because we do not have the detailed light curve through the rising phase, we cannot reject the scenario that the newly formed dust is being brought by a giant comet. However, the late cooling (on a timescale of years) is too slow for a departing comet. It is highly unlikely that the event was caused by a passing comet.

Grains spiral onto the host star due to radiation drag (the Poynting–Robertson drag) on a timescale of (Burn 1979; Backman & Paresce 1993)

$$t_{\rm PR} = 4.73\left(\frac{b}{1\mu m}\right)\left(\frac{\rho}{\rm g\ cm^{-3}}\right)^2\left(\frac{R}{R_\odot}\right)^2 \times\left(\frac{0.0035L_\odot}{L_{WD}}\right)\frac{1}{1+\rm albedo}{\rm yr}, \quad (4)$$

i.e., a few years in this case. Destruction of a large grain into small ones through collisions takes place on a timescale of (Backman & Paresce 1993)

$$t_{\rm col} = 3.5\left(\frac{R}{R_\odot}\right)^{3/2}\left(\frac{0.667M_\odot}{M_{\rm WD}}\right)^{1/2}\left(\frac{10^{-5}L_\odot}{L_{\rm IR}}\right){\rm yr}, \quad (5)$$

which is long, ~ 10 yr for the quiescent dust disk. Accretion of dust due to friction in the dust disk is much longer than 10^4 yr (Rafikov 2011; Girven et al. 2012). Given that this outburst event timescale appears to be consistent with the radiation drag and collision dust destruction timescales, it is most likely that the dust is produced by tidal breakup of an asteroid-like object.

The MIR observations are consistent with this picture. The temperature in the initial rising phase is as high as 1770 K in the blackbody fit. Assuming the dust is in radiative equilibrium, we estimate the distance of the dust to the WD is about $(0.63\pm 0.05)\,R_\odot$, which is consistent within a tidal disruption radius, $r_t = 0.69\left(\frac{M_{\rm WD}}{0.667M_\odot}\frac{3{\rm g\ cm^{-3}}}{\rho}\right)^{1/3}R_\odot$ of a gravitationally bounded asteroid with a typical density of $\rho = (1-7)\,{\rm g\ cm^{-3}}$ (Carry 2012). The disrupted debris will have a range of specific energies and will be spread in space. A small fraction with the lowest energies may fall directly onto the WD, and pollute the surface of the WD. A large part of debris may form an eccentric disk. Collision in the clump of debris will further cause fragmentation, releasing smaller grains, and thus increases the surface area of dust as observed. Similar events were detected before, for instance, evidence for planetesimals in an orbit close to the tidal disruption radius was reported in WD 1145+017 through the transit signal (Vanderburg et al. 2015; Xu et al. 2016). More recently, Manser et al. (2019) reported detection of a planetesimal orbiting within the debris disk through its perturbation to the gas disk. Farihi et al. (2018) proposed that dust production and depletion through collisions (secular evolution) are common based on the detection of MIR variability of 20% peak-to-peak amplitude over 11 yr in GD 56. Their light curve looked rather smooth. Xu et al. (2018) explored three mechanisms, including tidal disruption events, external perturbation, and runaway accretion, but did not reach a conclusion. The abrupt change in our object, on the other hand, suggests a catastrophic event. Our discovery may be the first case of an asteroid breakup process caught in action.

4. Conclusion and Perspective

We report a large MIR outburst of the WD 0145+234, which is still rising in the *WISE W2* band. We interpret this event as tidal disruption of an asteroid by the WD. As the source MIR flux is still rising, further monitoring of this event will likely help provide insights to the fate of planet systems at their end of star lives. High resolution spectroscopic observations in the optical and UV can trace the composition of recent falling debris (asteroid; e.g., Swan et al. 2019b). According to the calculation given by Fontaine,[18] the diffusion time for most metals are less than a month. The disruption may also release volatile gas into the interplanetary space, leaving absorption lines in the UV and optical spectra (Wilson et al. 2019). The debris may contain warm gas emitting infrared Ca II emission lines, which can be used to trace the kinematic motion of the debris. Infrared photometric observations at long wavelengths and MIR spectroscopy can be also used to constrain dust composition.

We thank the referee for constructive comments. This work is supported by Chinese Science Foundation (NSFC-11833007, 11421303). This research makes use of data products from the *Wide-field Infrared Survey Explorer*, which is a joint project of the University of California, Los Angeles, and the Jet Propulsion Laboratory/California Institute of Technology, funded by the National Aeronautics and Space Administration. This research also makes use of data products from NEOWISE-R, which is a project of the Jet Propulsion Laboratory/California Institute of Technology, funded by the Planetary Science Division of the National Aeronautics and Space Administration. This research has made use of the NASA/ IPAC Infrared Science Archive, which is funded by the National Aeronautics and Space Administration and operated by the California Institute of Technology.

ORCID iDs

Ting-gui Wang https://orcid.org/0000-0002-1517-6792
Ning Jiang https://orcid.org/0000-0002-7152-3621
Roc M. Cutri https://orcid.org/0000-0002-0077-2305
Peng Jiang https://orcid.org/0000-0002-5387-7952
Zhengfeng Sheng https://orcid.org/0000-0001-6938-8670
Hongyan Zhou https://orcid.org/0000-0003-1956-9021
Edward L. Wright https://orcid.org/0000-0001-5058-1593

[18] http://montrealwhitedwarfdatabase.org/evolution.html

References

Alexander, K. D., Berger, E., Guillochon, J., Zauderer, B. A., & Williams, P. K. G. 2016, ApJL, 819, L25
Backman, D. E., & Paresce, F. 1993, in Protostars and Planets III, ed. E. H. Levy & J. I. Lunine (Tucson, AZ: Univ. Arizona Press), 1253
Bergeron, P., Rolland, B., Limoges, M.-M., et al. 2015, in ASP Conf. Ser. 493, 19th European Workshop on White Dwarfs, ed. P. Dufour et al. (San Francisco, CA: ASP), 33
Bergeron, P., Wesemael, F., Dufour, P., et al. 2011, ApJ, 737, 28
Blouin, S., Dufour, P., & Allard, N. F. 2018, ApJ, 863, 184
Burn, I. 1979, JMatS, 14, 2453
Cardelli, J. A., Clayton, G. C., & Mathis, J. S. 1989, ApJ, 345, 245
Carry, B. 2012, P&SS, 73, 98
Chambers, K. C., Magnier, E. A., Metcalfe, N., et al. 2016, arXiv:1612.05560
Drake, A. J., Djorgovski, S. G., Mahabal, A., et al. 2009, ApJ, 696, 870
Farihi, J., Jura, M., & Zuckerman, B. 2009, ApJ, 694, 805
Farihi, J., van Lieshout, R., Cauley, P. W., et al. 2018, MNRAS, 481, 2601
Fontaine, G., Brassard, P., & Bergeron, P. 2001, PASP, 113, 409
Gaia Collaboration, Brown, A. G. A., Vallenari, A., et al. 2016, A&A, 595, A2
Gaia Collaboration, Brown, A. G. A., Vallenari, A., et al. 2018, A&A, 616, A1
Gänsicke, B. T., Marsh, T. R., Southworth, J., et al. 2006, Sci, 314, 1908
Gianninas, A., Bergeron, P., & Ruiz, M. T. 2011, ApJ, 743, 138
Girven, J., Brinkworth, C. S., Farihi, J., et al. 2012, ApJ, 749, 154
Jura, M. 2003, ApJL, 584, L91
Jura, M., Farihi, J., & Zuckerman, B. 2007, AJ, 133, 1927
Jura, M., & Young, E. D. 2014, AREPS, 42, 45
Kochanek, C. S., Shappee, B. J., Stanek, K. Z., et al. 2017, PASP, 129, 104502
Koester, D. 2009, A&A, 498, 517
Koester, D., Provencal, J., & Gänsicke, B. T. 2014, A&A, 568, A118
Laor, A., & Draine, B. T. 1993, ApJ, 402, 441
Limoges, M.-M., Bergeron, P., & Lépine, S. 2015, ApJS, 219, 19
Lindegren, L., Hernández, J., Bombrun, A., et al. 2018, A&A, 616, A2
Mainzer, A., Bauer, J., Cutri, R. M., et al. 2014, ApJ, 792, 30
Manser, C. J., Gänsicke, B. T., Eggl, S., et al. 2019, Sci, 364, 66
Nakamura, R. 1998, EP&S, 50, 587
Rafikov, R. R. 2011, MNRAS, 416, L55
Reach, W. T., Kuchner, M. J., von Hippel, T., et al. 2005, ApJL, 635, L161
Rebassa-Mansergas, A., Solano, E., Xu, S., et al. 2019, MNRAS, 489, 3990
Shappee, B. J., Prieto, J. L., Grupe, D., et al. 2014, ApJ, 788, 48
Skrutskie, M. F., Cutri, R. M., Stiening, R., et al. 2006, AJ, 131, 1163
Swan, A., Farihi, J., Koester, D., et al. 2019a, MNRAS, 490, 202
Swan, A., Farihi, J., & Wilson, T. G. 2019b, MNRAS, 484, L109
Tremblay, P.-E., Bergeron, P., & Gianninas, A. 2011, ApJ, 730, 128
Vanderburg, A., Johnson, J. A., Rappaport, S., et al. 2015, Natur, 526, 546
Veras, D., Leinhardt, Z. M., Bonsor, A., et al. 2014, MNRAS, 445, 2244
Wills, D., & Wills, B. J. 1974, MNRAS, 167, 79P
Wilson, D. J., Gänsicke, B. T., Koester, D., et al. 2019, MNRAS, 483, 2941
Wright, E. L., Eisenhardt, P. R. M., Mainzer, A. K., et al. 2010, AJ, 140, 1868
Xu, S., & Jura, M. 2014, ApJL, 792, L39
Xu, S., Jura, M., Dufour, P., et al. 2016, ApJL, 816, L22
Xu, S., Su, K. Y. L., Rogers, L. K., et al. 2018, ApJ, 866, 108
Zuckerman, B., & Becklin, E. E. 1987, Natur, 330, 138
Zuckerman, B., Melis, C., Klein, B., et al. 2010, ApJ, 722, 725